JOURNAL OF GEOPHYSICAL RESEARCH, VOL. 115, B04103, doi:10.1029/2009JB006703, 2010

Reliability of the natural remanent magnetization recorded in Chinese loess

Chunsheng Jin[1] and Qingsong Liu[1]

Received 3 July 2009; revised 31 October 2009; accepted 19 November 2009; published 23 April 2010.

[1] Chinese loess-paleosol sequences undoubtedly have recorded geomagnetic events (both polarity reversals and excursions). However, the fidelity of the rapid paleomagnetic field oscillations during a polarity reversal remains uncertain. To test the reliability and consistency of the natural remanent magnetization records in Chinese loess, 10 subsets of parallel samples across the Matuyama-Brunhes (MB) reversal boundary were obtained from the Luochuan region in the hinterland of the Chinese Loess Plateau. Our paleomagnetic results show diversified virtual geomagnetic poles (VGPs) during the MB transition but consistent VGPs outside of the transitional zone. The anisotropy of magnetic susceptibility and rock magnetism results indicate that the sampled interval is rather uniform and undisturbed. The discrepancies of the characteristic remanent magnetization within the MB transition are probably due to the low efficiency in aligning magnetic grains, mainly pseudo-single-domain magnetite, associated with the low field intensity. Nevertheless, the stratigraphic location of the MB boundary can be confidently defined. Therefore, we conclude that Chinese loess-paleosol sequences can record geomagnetic reversal events, but the morphology within the polarity transition is rather questionable.

Citation: Jin, C., and Q. Liu (2010), Reliability of the natural remanent magnetization recorded in Chinese loess, *J. Geophys. Res.*, *115*, B04103, doi:10.1029/2009JB006703.

1. Introduction

[2] Windblown deposits in northwest China, mainly on the Chinese Loess Plateau (CLP), with an approximate area of 440, 000 km^2, are one of the most continuous terrestrial sediments [*Liu*, 1985]. Loess-paleosol sequences formed during glacial and interglacial periods, respectively, can be dated back to the late Pliocene [*Heller and Liu*, 1984] or even to the Miocene [*Guo et al.*, 2002b]. Previous studies have shown that they are excellent archives of paleoclimate at different timescales, which can be correlated well with records of marine sediments and ice cores [*Heller and Liu*, 1986; *Porter and An*, 1995; *Ding et al.*, 2002]. In addition, paleomagnetic signals recorded by Chinese loess have been extensively studied [*Heller and Liu*, 1982; *Heller and Evans*, 1995; *Evans and Heller*, 2001], including both main geomagnetic reversals, such as the Gsuss-Matuyama reversal [*Zhu et al.*, 2000a] and Matuyama-Brunhes (MB) reversal [*Sun et al.*, 1993; *Zhu et al.*, 1993, 1994a; *Guo et al.*, 2001; *Spassov et al.*, 2001], and some polarity subchrons, such as the Upper Jaramillo boundary [*Guo et al.*, 2002a] and Upper Olduvai boundary [*Yang et al.*, 2008], and short geomagnetic events and excursions [*Zhu et al.*, 1994b, 1999, 2006, 2007; *Zheng et al.*, 1995; *Fang et al.*, 1997; *Pan et al.*, 2002; *Yang et al.*, 2004].

[3] The paleomagnetic results provide not only the first chronology framework for the long loess-paleosol sequences, but also strong constraints for the geodynamic processes occurring in the Earth's interior. Among these records, the MB reversal has been well studied [*Zhu et al.*, 1993, 1994a; *Sun et al.*, 1993; *Guo et al.*, 2001; *Spassov et al.*, 2001], but there remain some inconsistencies in the MB reversal records from different sites in terms of stratigraphic location, duration, and morphology of the transition field.

[4] First, the stratigraphic location of the MB boundary (MBB) remains uncertainty. Most studies have shown that the MBB is located in the lower part of loess unit L8 (corresponding to a glacial period [*Liu*, 1985]), for example, in Weinan [*Zhu et al.*, 1994a; *Pan et al.*, 2002], Lantian [*Zheng et al.*, 1992] (in the Xi'an area), Lingtai [*Ding et al.*, 1998; *Spassov et al.*, 2001], Pingliang [*Sun et al.*, 1998], Baoji [*Rutter et al.*, 1991; *Spassov et al.*, 2001; *Yang et al.*, 2004], Jingbian [*Ding et al.*, 1999; *Guo et al.*, 2002a], and Xifeng [*Liu et al.*, 1987; *Sun et al.*, 1993; *Zhu et al.*, 1993], with exceptions in Luochuan [*Heller and Liu*, 1982] and Sanmenxia [*Wang et al.*, 2005], where the MBB was located in paleosol unit S8 (corresponding to an interglacial period [*Liu*, 1985]). In marine sediments, the MBB was mostly located in MIS19, corresponding to an interglacial period [*Tauxe et al.*, 1996]. Therefore, *Zhou and Shackleton* [1999] proposed a large lock-in model (2–3 m in lock-in depth or 20–30 ka in lock-in time) for the paleomagnetic signals recorded by Chinese loess.

[5] Second, the depth of the MBB differs at different sites, ranging from tens to more than 200 cm, for example, 30 cm

[1]Paleomagnetism and Geochronology Laboratory, Institute of Geology and Geophysics, Chinese Academy of Sciences, Beijing, China.

0148-0227/10/2009JB006703

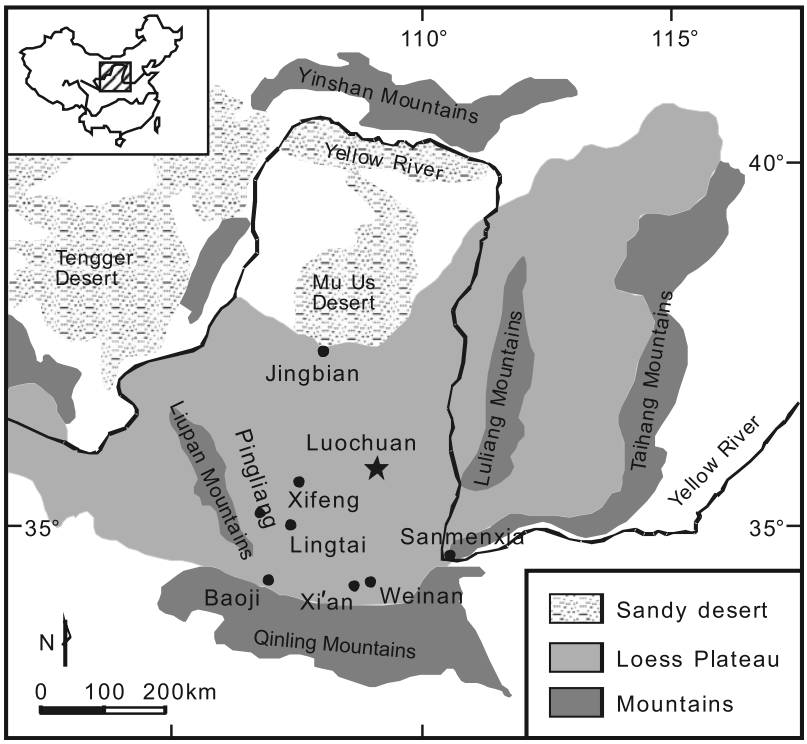

Figure 1. Location of the Chinese Loess Plateau. The star indicates the sampling site. Circles indicate other sections mentioned in the text.

in Duanjipo [*Guo et al.*, 2001], 36 cm in Xifeng [*Zhu et al.*, 1993], 40 cm in Lingtai [*Spassov et al.*, 2001], 50 cm in Sanmenxia [*Wang et al.*, 2006] and Weinan [*Zhu et al.*, 1994a], 78 cm in Baoji [*Yang et al.*, 2007], and 223.2 cm in Xifeng [*Sun et al.*, 1993].

[6] Third, the morphology of the transitional field within the MBB also exhibits inconsistent features. For example, the number of rapidly directional oscillations during the MB transition differs from site to site, for example, 5 in Xifeng [*Zhu et al.*, 1993], Weinan [*Zhu et al.*, 1994a], and Duanjiapo [*Guo et al.*, 2001] (in the Xi'an area), 7 in Lingtai [*Spassov et al.*, 2001], 9 in Sanmenxia [*Wang et al.*, 2006], and 15 in Baoji [*Yang et al.*, 2007]. In addition, the virtual geomagnetic pole (VGP) paths are also inconsistent among different records. In Xifeng the VGP paths during the MB transition prefer to follow longitude bands comprising America, the Atlantic Ocean, or Africa [*Sun et al.*, 1993]. Field behaviors during the transition period suggest that nondipole components were dominant, while the dipole field was weak [*Sun et al.*, 1993]. But records from another site in the Xifeng area show distinct features, with VGP positions during the MB transition being predominantly distributed around northern or southern poles and having intermediate positions when moving from one pole to another [*Zhu et al.*, 1993]. This phenomenon suggests that dipole field components were at least comparable in magnitude to nondipole ones during the MBB [*Zhu et al.*, 1993]. In Weinan VGP paths during the MB transition move along two longitudinal sectors situated over eastern Asia and Australia [*Zhu et al.*, 1994a]. In Duanjiapo section the VGP path is confined over Africa [*Guo et al.*, 2001].

[7] These inconsistencies have been attributed to lock-in effects of remanence acquisition associated with pedogenesis [*Zhou and Shackleton*, 1999; *Spassov et al.*, 2003], regional and/or local climate variability across the CLP [*Wang et al.*, 2006], an inaccurate paleoclimatic boundary between L8 and S8 [*Liu et al.*, 2008], pedogenic effects on VGP paths [*Guo et al.*, 2001], and so on. Because it is hard to simulate the natural depositional process and remanence acquisition process of eolian dust in the laboratory, there is still some lack of knowledge about the complexity of natural remanence acquisition of Chinese loess-paleosol. This complexity raises suspicion whether the rapid changes in the geomagnetic field during the MB reversal are faithfully preserved in Chinese loess-paleosol sequences [*Zhou and Shackleton*, 1999; *Guo et al.*, 2001; *Spassov et al.*, 2003].

[8] Most MBB results from Chinese loess were obtained from only one or two sets of samples and sometimes a rapid reversal interval is represented by only one specimen. To reduce the uncertainties in the records, in this study we investigate large numbers of parallel subspecimens of the MBB from the Luochuan section. We aim to test the reliability and consistency of paleomagnetic records during the MBB recorded in Chinese loess.

2. Sampling and Measurements

[9] The Luochuan section (35.7°N, 109.4°E), located in the hinterland of the CLP (Figure 1), northwest of China, involves 33 loess-paleosols about 120 m thick underlain by red clay more than 10 m thick. Samples were collected from loess unit L8 and the upper part of paleosol unit S8, which

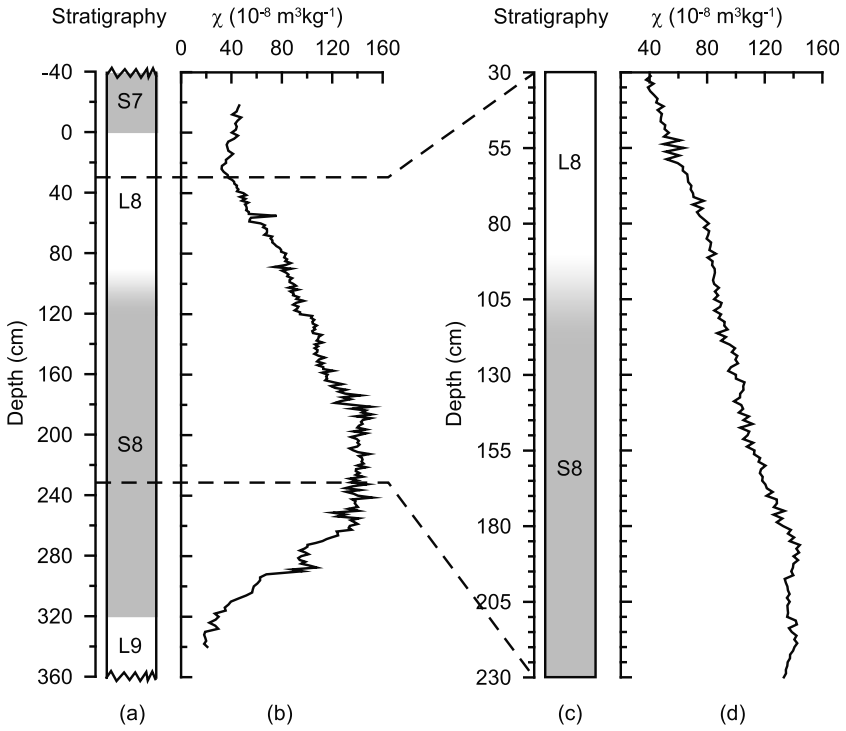

Figure 2. (a) Lithostratigraphy and (b) mass-specific low field magnetic susceptibility (from bulk samples) of the sampled Luochuan section spanning S7 to L9. S7 and S8 (L8 and L9) correspond to paleosol (loess). (c) Part of Figure 2a for block samples. (d) Low field mass-normalized magnetic susceptibility from oriented block specimens.

have an indistinct stratigraphic boundary between them. The total sampling thickness is about 200 cm (Figure 2).

[10] After removal of surface weathered material covering the outcrop, vertical faces were carved, along which block samples with a base of about 12 × 12 cm^2 and 30 cm in vertical height were continuously collected (Figure 3). All samples were oriented in situ using a magnetic compass, with the direction of north marked on the top surface.

[11] In the laboratory each block sample was divided vertically into two parts, A and B, with a 1.25-cm offset (Figure 3). Then parts A and B were cut into 2.5-cm-thick slices along the horizontal plane and oriented cube specimens of 2 × 2 × 2 cm^3 were taken from each slice [*Zhu et al.*, 1993]. We got seven parallel subsets from both part A (called sets A1–A7) and part B (sets B1–B7). A total of 672 oriented specimens were used for measurements. Sets A6 and B6 were used for low-field magnetic susceptibility (χ, mass-specific) measurements and determination of relative paleointensity (RPI). Ten sets of samples (sets A1–A5 and B1–B5) were used to obtain paleomagnetic field directions using thermal demagnetization. Set A7 was used for anhysteretic remanent magnetization (ARM) and isothermal remanent magnetization (IRM).

[12] The χ value was measured using a Bartington MS2 susceptibility meter. Temperature-dependent susceptibility (χ-T) curves were measured with a KLY-3s Kappabridge equipped with a CS-3 high-temperature furnace going from room temperature up to 700°C in an argon atmosphere to avoid magnetic mineral alteration upon heating. The anisotropy of magnetic susceptibility (AMS) was also measured with the KLY-3s Kappabridge.

[13] Hysteresis loops, IRM acquisition curves, back-field demagnetization curves, and temperature-dependent saturation magnetization (M_s-T curves) were measured for representative samples using a variable field translation balance

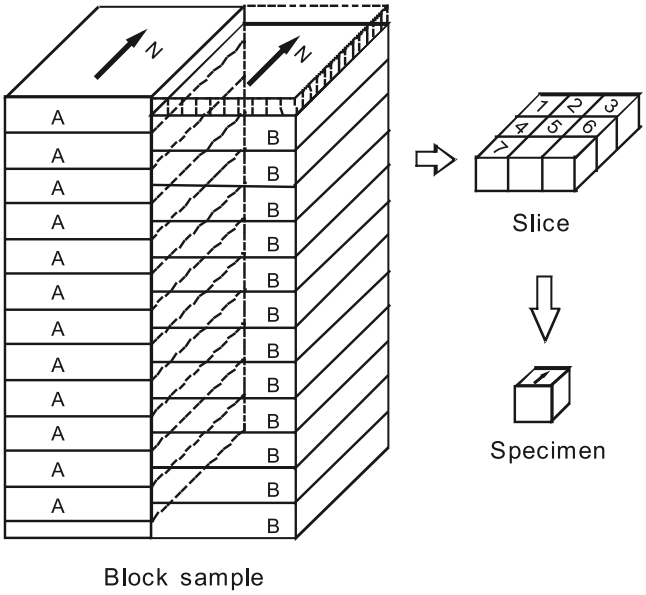

Figure 3. Schematic of sample processing. The block sample was vertically divided into two parts first. Then we sawed off the top 1.25 cm of part B. Parts A and B (without the top 1.25 cm) were sawn into slices 2.5 cm thick and, finally, oriented specimens of approximately 2 × 2 × 2 cm^3.

system. Samples for M_s-T curves were heated in an applied field of 1 T in air. The temperature sweeping rate was 40°C per minute. Hysteretic parameters, such as coercivity (B_c), saturation magnetization (M_s), and saturation remanence (M_{rs}) were obtained after subtraction of the paramagnetic contribution.

[14] ARM was imparted using an alternating field (AF) with a peak of 100 mT superimposed on a 0.05 mT DC-biased field using a Model 615 anhysteretic remanent magnetizer. Saturation IRM (SIRM) was acquired in a DC field using a 2G660 pulse magnetizer with 1.5 and 300 mT back fields for calculating the S ratio (defined as $-IRM_{-0.3T}$/SIRM) and hard IRM (defined as 0.5 × (SIRM + $IRM_{-0.3T}$)).

[15] Progressive thermal demagnetization was performed on 432 specimens from room temperature up to 680°C in steps of 10°–50°C using a Magnetic Measurements Thermal Demagnetizer (MMTD80) with a residual magnetic field of <10 nT. All remanences were measured using a 2G Enterprises model 760 cryogenic magnetometer installed in a magnetically shielded room (<300 nT).

3. Rock Magnetic Results

3.1. Thermomagnetic Analyses

[16] The χ-T curve is highly sensitive to changes in magnetic minerals during thermal treatments. Therefore, it has been widely used as a routine rock magnetic tool to identify magnetic mineralogy and possible mineral transformation upon heating. The χ-T curves for representative samples (Figures 4a–4d) exhibit a major decrease in susceptibility at about 585°C, displaying the Curie point of magnetite. At lower temperatures (<280°C) the susceptibility increases slowly owing to the unblocking of single-domain phases [*Liu et al.*, 2005b; *Deng et al.*, 2005, 2006; *Deng*, 2008]. Above 280°C the susceptibility decreases steadily, which is generally interpreted as the conversion of metastable maghemite to weakly magnetic hematite [*Liu et al.*, 2005b; *Deng et al.*, 2000, 2004, 2005, 2006; *Deng*, 2008].

[17] Another notable feature of the χ-T curves is that they are nearly irreversible after about 570–590°C when cooling. The susceptibility after cooling is several times higher than the initial value of samples at room temperature, which is generally attributed to the neoformation of magnetite grains from iron-containing silicates/clays or due to the formation of magnetite by reduction owing to the burning of organic matter [*Liu et al.*, 2005b; *Deng*, 2008].

[18] The M_s-T curve is generally preferred for determining the Curie temperature of natural samples. It is irreversible for M_s-T curves during heating and cooling, with identifiable signals of paramagnetic contributions at high temperature (Figures 4e–4h). The decrease in M_s at about 580°C upon heating further suggests the Curie point of magnetite, indicating the presence of magnetite. The slight kick between about 300 and 500°C is generally identified as the existence of metastable maghemite, which could transform easily to hematite in this temperature interval [*Liu et al.*, 2003].

3.2. Isothermal Remanent Magnetization Acquisition and DC-Field Demagnetization Curves

[19] IRM acquisition and back-field demagnetization of SIRM were carried out on the selected five samples to identify magnetic minerals further. They show shape similarity of the acquisition curves (Figure 5a), which rise steeply in the initial stages and reach 80% of the SIRM (here imparted by 1 T) before 300 mT. The IRM continues to climb slowly after 300 mT and does not reach full saturation until 1 T. These characteristics indicate that soft magnetic components of low coercivity (e.g., magnetite and maghemite) dominate the IRM, with the coexistence of a hard magnetic portion (e.g., hematite, probably goethite) for both L8 and S8. SIRM is higher for S8 than for L8 (Figure 5a).

[20] The stepwise demagnetization of SIRM using a DC back field shows a lower coercivity of remanence (B_{cr}) for S8 (27.1 and 25.4 mT for two selected samples) than for L8 (43.2, 31.7, and 31.8 mT for the other three selected samples) (Figure 5b).

3.3. Hysteresis Properties

[21] Hysteresis loops after subtracting the paramagnetic contribution for the representative samples from L8 and S8 display a weakly wasp-waisted shape representing a mixed nature of magnetic minerals with low and high coercivity (Figure 6). They are closed at about 310, 300, 280, and 250 mT (Figures 6a–6d, respectively), indicating a decrease in the magnetically hard component depending on the enhancement of pedogenesis. Meanwhile, B_c (from 11.7 to 7.5 mT) and B_{cr} (from 43.2 to 25.4 mT) decrease depending on the enhancement of pedogenesis, contrary to the increase in M_s and M_{rs} (see Figure 6).

[22] Hysteresis parameter ratios (M_{rs}/M_s, B_{cr}/B_c) were plotted on a Day plot [*Day et al.*, 1977; *Dunlop*, 2002] to determine the domain state of magnetic minerals in samples (Figure 6e). All plots are constrained in a pseudo-single-domain (PSD) area and cluster closely. This indicates that samples from Brunhes, a transitional zone, and Matuyama are similar in mean magnetic grain size.

3.4. Anisotropy of Magnetic Susceptibility Analysis

[23] In previous loess studies, AMS results, especially the inclination of the maximum-susceptibility axis (K_{max}-Inc) and minimum-susceptibility axis (K_{min}-Inc), have been widely used to detect possible disturbance of the original sediment fabric [e.g., *Liu et al.*, 1988; *Zhu et al.*, 1999; *Guo et al.*, 2001, 2002a; *Liu et al.*, 2005a; *Wang et al.*, 2005; *Yang et al.*, 2008]. The K_{max}-Inc, K_{min}-Inc, P, and T of sets A5 and B5 throughout the sampled interval are shown in Figures 7c–7f. The susceptibility ellipsoid is oblate shaped ($T < 1$; Figure 7f) and K_{max}-Inc is less than 15° (97% < 10°) (Figure 7c), perpendicular to the vertical plane, whereas K_{min}-Inc is larger than 72° (Figure 7d), suggesting a primary sediment fabric without apparent disorder or disturbance. P (<1.016) is obviously less than 1.032, which has been suggested as the critical cutoff between redeposited loess and original loess by *Liu et al.* [1988], further indicating an original fabric (Figure 7e).

[24] We further measured the AMS of 10 sets of samples in the interval of 66.25–150 cm (shown in Figure 8). The mean declinations of the maximum, intermediate, and minimum axes are 165°, 255°, and 3°, respectively. The mean inclinations of the maximum, intermediate, and minimum axes are 3°, 1°, and 87°, respectively. K_{max} directions are approximately parallel to the horizontal plane, with an inclination generally less than 10°, perpendicular to the

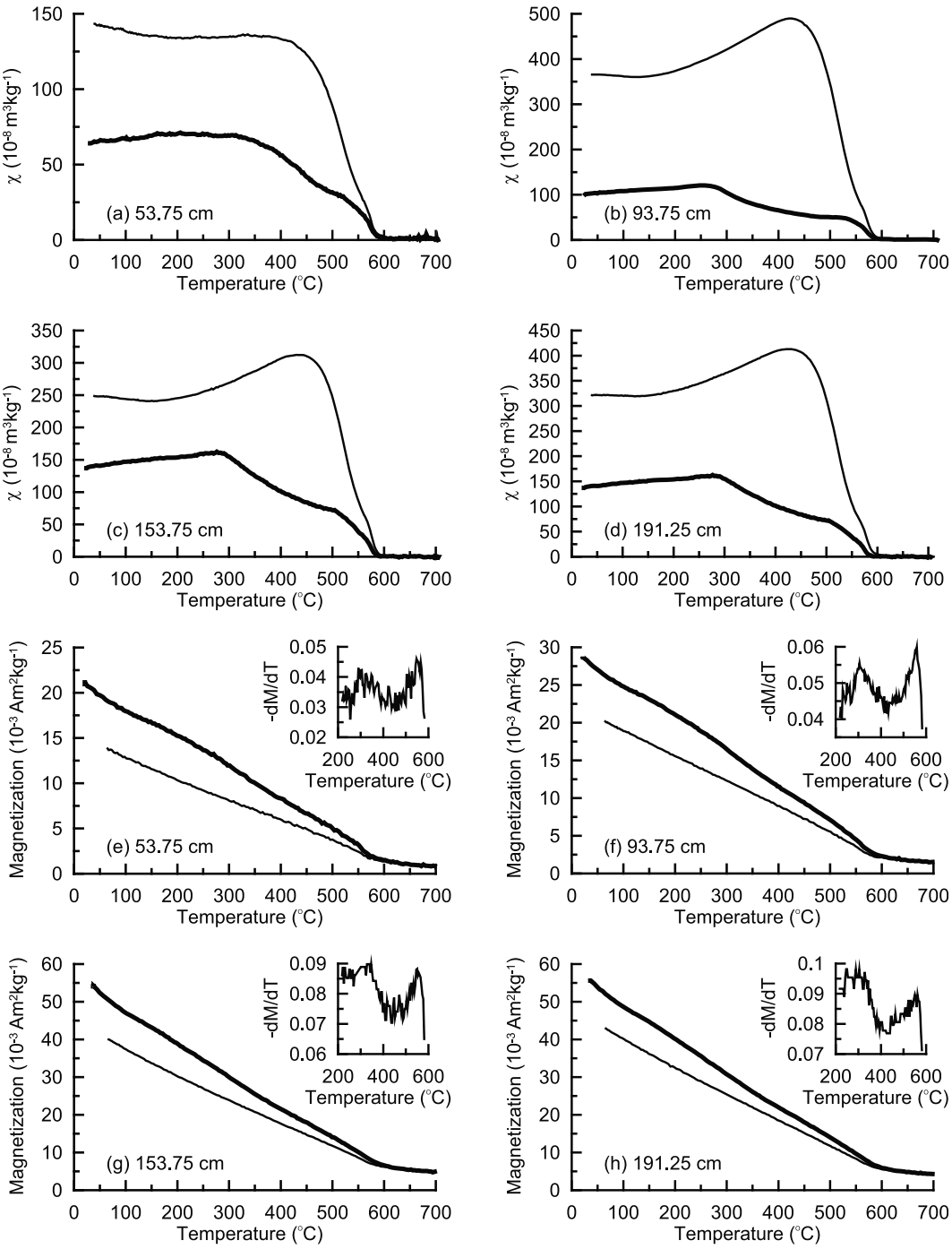

Figure 4. Temperature dependence of (a–d) magnetic susceptibility and (e–h) high-temperature magnetization for representative samples. Samples are (a, b, e, f) from L8 and (c, d, g, h) from S8. Thicker lines indicate heating runs. $-dM/dT$ (10^{-3} Am^2 kg^{-1} T^{-1}) indicates the first derivative of M_s-T curves.

vertical plane, whereas K_{min}-Inc is approximately vertical, also indicating a primary sediment fabric.

4. Paleomagnetic Results

4.1. Paleomagnetic Directions

[25] The initial natural remanent magnetization (NRM) directions of samples (D = 344.9°, I = 49.7°, n = 432, α_{95} = 0.7°) represent normal polarity close to the present geomagnetic field value at the sampling site. About 80%–90% of the initial NRM was demagnetized after thermal treatment at 250–300°C. Low-temperature NRM components are viscous remanent magnetization (VSM) [*Heller and Liu*, 1984; *Pan et al.*, 2001; *Guo et al.*, 2002a]. Characteristic remanent magnetization (ChRM) was defined between 300 and 500°C. Principal component analysis, calculated by a least-squares fitting technique [*Kirschvink*, 1980] was carried out on demagnetization data using the PaleoMag

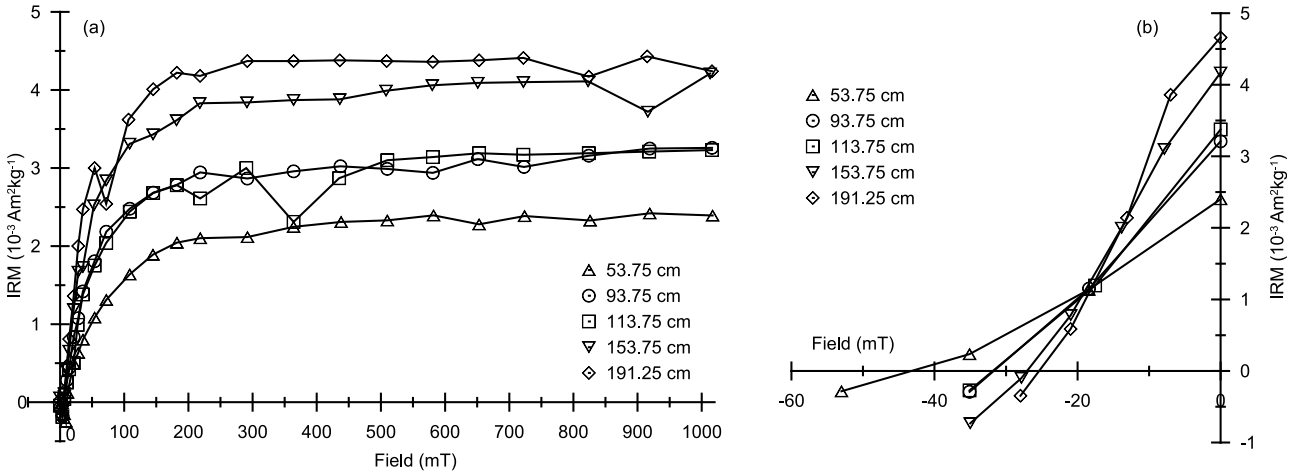

Figure 5. (a) Isothermal remanent magnetization (IRM) acquisition curves and (b) back-field demagnetization of saturation IRM for representative samples.

software (version 3.1d40) developed by Craig H. Jones and Joya Tetreault, University of Colorado at Boulder. Generally, we consider mean directions of ChRM with a angle deviation of <15° to be reliable results.

[26] Orthogonal projections of 20 representative specimens are shown in Figure 9. Samples at 71.25 cm (Figures 9a–9e, normal), 81.25 cm (Figures 9f–9j, transitional zone), and 115 cm (Figures 9k–9o, transitional zone) are from L8, and those at 130 cm (Figures 9p–9t, reverse) are from S8. There are five specimens from the same depth level. It is clearly shown that the orthogonal vector for the five specimens outside the transitional zone at 71.25 and 130 cm are perfectly consistent with each other. Almost all specimens outside the MBB showed stable ChRM. In contrast, no consistent ChRM was obtained within the transitional zone. For instance, five specimens at 81.25 cm show different results: two show normal polarity (Figures 9f and 9g), two show reverse polarity (Figures 9h and 9i), and one shows scattered directions after 300°C where stable ChRM cannot be gained (Figure 9j). This is more complex for specimens at 115 cm. Two specimens represent reverse polarity (Figures 9l and 9n), and one shows normal polarity (Figure 9o). Two specimens carry unstable ChRM (Figures 9k and 9m). Within the transitional zone, only 123 (68%) specimens gave stable ChRM.

[27] VGP latitudes (VGP Lat) were calculated after evaluation of ChRM vector directions. Paleomagnetic results for set A5, associated with set B5, are shown in Figures 7i–7l. There is an obvious paleomagnetic polarity transition from Matuyama reverse polarity to Brunhes normal polarity, with a transitional zone of 27.5 cm over 90–117.5 cm, rather than a single reversal. Several rapid changes in paleomagnetic direction occur during transition, resembling results of previous studies [e.g., *Sun et al.*, 1993; *Zhu et al.*, 1993, 1994a; *Guo et al.*, 2001; *Spassov et al.*, 2001; *Wang et al.*, 2006; *Yang et al.*, 2007].

[28] To test the reliability of the rapid directional changes during the MBB in L8, thermal demagnetization was carried out on parallel samples in the interval 66.25–150 cm. Paleomagnetic results for sets A1–A4 and B1–B4, along with sets A5 and B5 at 66.25–150 cm, are shown in Figure 10. The transitional zone of the MBB extends to 47.5 cm between 73.75 and 121.25 cm. *Fisher* [1953] statistics were applied to parallel samples with stable ChRM to calculate the mean values over the depth intervals 6.25–73.75 cm (D = 355.0°, I = 45.8°, n = 35, α_{95} = 5.2°), 73.75–121.25 cm (D = 348.1°, I = 48.4°, n = 123, α_{95} = 10.4°), and 121.25–150 cm (D = 180.2°, I = −45.4°, n = 118, α_{95} = 1.6°). Statistical results show that samples within the transitional zone have more scattered ChRM than those outside the transitional zone. Additionally, it is hard to obtain statistical data from the five parallel specimens within the MBB in the same slice (Figures 10r, 10u, 10x, 10aa, and 10ad and Figures 10c, 10f, 10i, 10l, and 10o), partly because of the lack of stable ChRM for all five specimens and partly because of the dispersion of VGP paths for the samples with stable ChRM at the same level (VGP Lat in Figure 10). So statistical analysis [*Fisher*, 1953] was performed on 10 subsets of parallel samples with depth resolution at 2.5 cm intervals to define the dispersion of ChRM indicated by error bars (expressed as α_{95}) (Figures 10ae–ag). Clearly, error bars within the MBB are much larger than those outside the MBB. There is also diversity between adjacent sets with a 1.25 cm difference in vertical depth, such as sets A1 and B1, sets A2 and B2, sets A3 and B3, sets A4 and B4, and sets A5 and B5.

4.2. Relative Paleointensity

[29] The RPI of sediments is significant in discussing paleomagnetic field evolution and is also used as an independent timescale [e.g., *Guyodo and Valet*, 1999; *Valet et al.*, 2005]. It is often constructed by normalization of NRM to some rock magnetic parameters, generally χ, ARM, and SIRM, to eliminate the contributions of nonmagnetic effects, especially concentration of magnetic grains in samples [*Levia and Banerjee*, 1976; *Tauxe*, 1993; *Valet*, 2003]. A pseudo-Thellier method was also used for construction of the RPI, which has advantages for estimating uncertainties [*Tauxe et al.*, 1995]. A large number of RPI records were gained from marine and lacustrine sediments as well as Chinese loess.

[30] Rock magnetism results indicate that magnetite is the dominant magnetic carrier of remanence in this study (shown in Figures 4–6). The S ratio is nearly constant, with

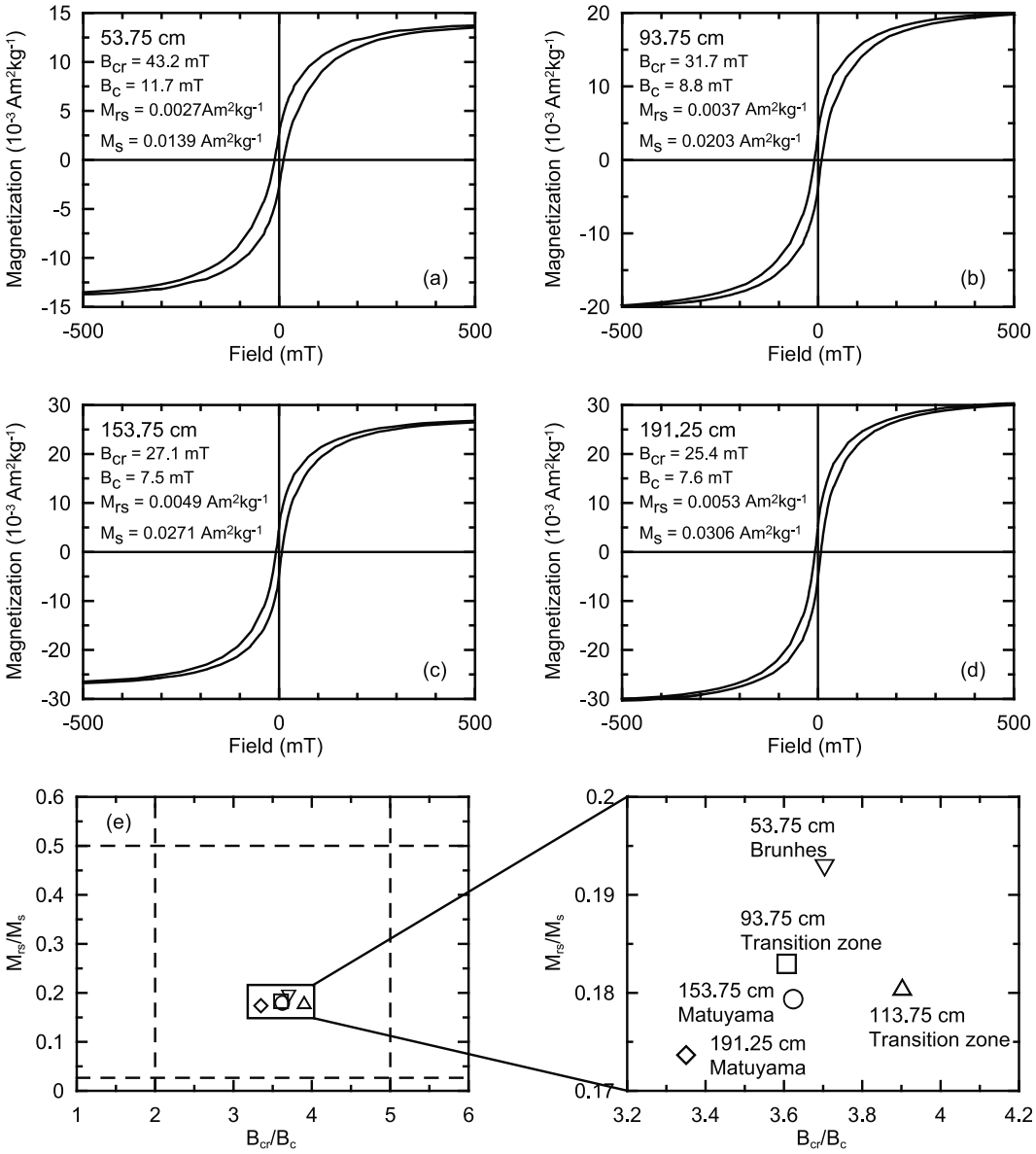

Figure 6. (a–d) Magnetic hysteresis loops (after correction of paramagnetic contribution) for selected samples. (e) Hysteresis ratios plotted on a Day plot [*Day et al.*, 1977; *Dunlop*, 2002].

an average value of 0.87, also suggesting that magnetite is dominant in sampled sections (Figure 7g). The Day plot (Figure 6e) suggests that the magnetic grain size is approximately uniform, with constraint within the PSD range. Sampled sections are characterized by uniformity of magnetic grain size and ChRM carriers and low variation in the concentration of magnetic mineralogy, which are required for reliable RPI estimates [*Tauxe*, 1993]. It is feasible to construct the RPI with our samples.

[31] Here we followed the methods of *Pan et al.* [2001] with some modifications to construct the RPI around the MB reversal. Sets A6 and B6 (total of 160 specimens) were used for RPI in the following procedure. First, χ was measured. Second, samples were treated with 300°C thermal demagnetization followed by AF demagnetization with a peak of 100 mT (AF, 100 mT). Then ARM was imparted with an AF of 100 mT superimposed on a 0.05 mT DC field. ARM was treated with 300°C thermal demagnetization and then another AF of 100 mT demagnetization. Third, χ was measured again to observe mineralogy changes. SIRM was imparted with a 1.5 T DC field and then another 300°C thermal demagnetization. Finally, we measured χ for the third time. We refer to NRM, ARM, and SIRM after 300°C thermal demagnetization as NRM300, ARM300, and SIRM300. In fact, χ values before NRM and after NRM300 and ARM 300 were approximately consistent, indicating that mineralogy conversion during thermal treatments was too weak to affect RPI. The pseudo-Thellier method is not suitable here because the reverse ChRM of selected tentative samples with reverse polarity proved by thermal demagnetization cannot be isolated by AF demagnetization, even with a peak AF of 150 mT (results not shown here). This behavior indicates that the viscous NRM components of samples may be carried not only by ferromagnetic minerals

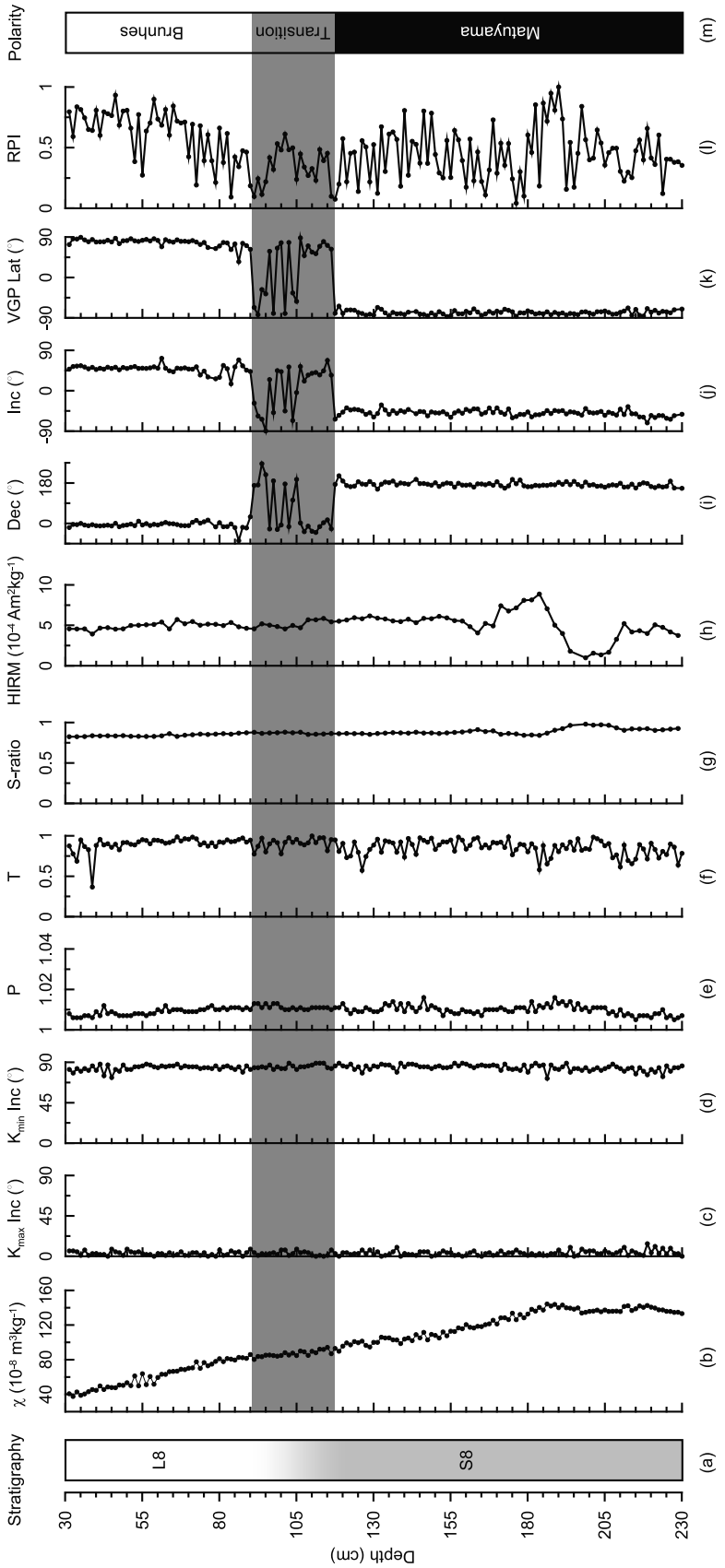

Figure 7. (a) Stratigraphy for sampled interval; (b) low field susceptibility; (c) inclination of maximum-susceptibility axis (K_{max}); (d) inclination of minimum-susceptibility axis (K_{min}); (e) degree of anisotropy of magnetic susceptibility (AMS); (f) AMS ellipsoid shape; (g) *S*-ratio; (h) hard IRM (HIRM); (i) declination (Dec) of characteristic remanent magnetization (ChRM); (j) inclination (Inc) of ChRM; (k) virtual geomagnetic pole latitude (VGP Lat); (l) relative paleointensity (RPI); (m) magnetic polarity. The transitional interval of paleomagnetic directions is shaded.

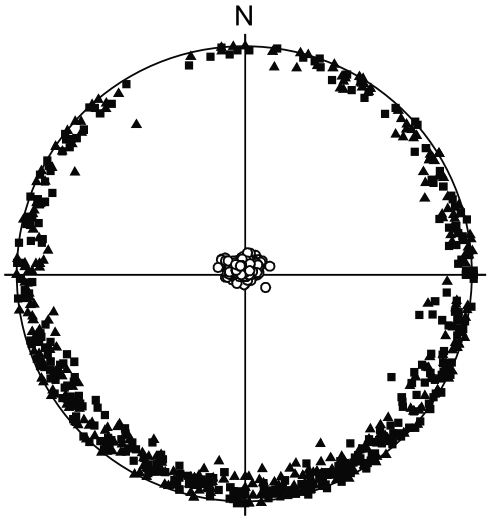

Figure 8. AMS principal directions in an equal-area stereographic projection for 10 sets of samples in the interval 66.25–150 cm. Total number of samples was 340. Squares, triangles, and circles represent K_{max}, K_{int}, and K_{min}, respectively.

but also by high-coercivity ones [*Heller et al.*, 1987] that cannot be eliminated by AF demagnetization. In addition, this behavior may be attributed to low-temperature oxidation, which can significantly increase the coercivity of coarser-grained partially oxidized magnetites [*Liu et al.*, 2004, 2005a].

[32] The ratios NRM300/SIRM300, NRM300/ARM300, and NRM300/χ were normalized by the peak value of each sequence. The first-order feature shown in Figure 11 is that the trends of the three curves are in agreement. Overall, the RPI begins with a slight increase from the bottom of the stratigraph to 195 cm, then decreases with a weak trend to about 90–110 cm, with two small peaks at about 140 and 190 cm (Figure 11a). The RPI increases rapidly at 90 cm and reaches a peak at about 35 cm. The low RPI values correlate with rapid directional changes in the MB reversal (Figures 7i–7l and 11). The RPI decays earlier than the directional changes and requires more time to recover, which is consistent with previous studies [*Zhu et al.*, 1994a]. Changes in RPI are characterized asymmetrically, with a pretransitional field strength significantly weaker than the posttransitional field strength, which recovers more rapidly than the decay.

[33] In addition, samples in or out of the transitional zone maintain the same AMS characteristics (Figures 7c–7f), indicating that the paleomagnetic direction abnormality at 73.75–121.25 cm (Figure 10) and the low RPI during reversal (Figure 11) were not caused by sedimentary disturbances (e.g., bioturbation and slumping) or mistakes in field sampling or in the laboratory.

5. Discussion

[34] Previous studies on various media (lava flows, marine and lacustrine sediments) have demonstrated that the MBB is characterized by some rapidly oscillating features, which may partly represent the evolution of geomagnetic dynamics [e.g., *Valet et al.*, 1988; *Tauxe et al.*, 1992; *Oda et al.*, 2000; *Yamazaki and Oda*, 2001; *Channell et al.*, 2004; *Coe et al.*, 2004; *Hyodo et al.*, 2006]. Although directional oscillations of the paleomagnetic field during the MBB in Chinese loess were undoubtedly recorded and the MBB has been used to construct the first-order loess chronological framework, the morphology of the transitional field within the MBB differs greatly from site to site [e.g., *Yue et al.*, 1990; *Ma et al.*, 1991; *Sun et al.*, 1993; *Zhu et al.*, 1993, 1994a; *Guo et al.*, 2001; *Spassov et al.*, 2001; *Wang et al.*, 2006; *Yang et al.*, 2007]. Correlation between sections cannot be employed as a common criterion to test the reliability of paleomagnetic recording because windblown sediments may not be continuous over a short timescale (e.g., millennial scale) [*Zhu et al.*, 2007; *Deng*, 2008]. A more feasible approach is to test the reproducibility of the NRM records within a limited horizon level by using large numbers of parallel specimens.

[35] Our results clearly show that the ChRM for parallel samples within the MBB is rather scattered, partly due to the failure to obtain stable ChRM. ChRMs of 10 sets of samples are not consistent with one another (shown by shading in Figure 10). For instance, almost one third of specimens within the transition did not record stable ChRM. In this case, it is hard to treat the high-frequency features faithfully as a reliable record. Therefore, some of the high-resolution paleomagnetic records from the CLP [e.g., *Guo et al.*, 2001; *Yang et al.*, 2007, 2008] would have been more convincing if parallel specimens had been examined, especially for those paleodirectional anomalies defined by only one sample. The distinct discrepancies in the number of rapid directional changes during the MB reversal in other loess sections are indirect evidence supporting our suspicion of the capability of loess to record millennium- or century-scale rapid changes in paleomagnetic field within the reversal. In fact, such a pattern has also been observed in other regions, for example, in the Tecopa basin, southeastern California, USA, where four sampling sites distributed over a small area revealed diverse transitional processes, and none of these records provided an acceptable record of the MB transition [*Hillhouse and Cox*, 1976; *Valet et al.*, 1988; *Larson and Patterson*, 1993].

[36] However, AMS and rock magnetic results both indicate that the whole sequence is rather uniform and undisturbed. Therefore, the diversified records within the MBB are not due to the depositional or postdepositional environment. One plausible mechanism is due to the low efficiency in aligning magnetic grains associated with the low field intensity during the MB reversal. It is well accepted that polarity reversals always correspond to a low field intensity [e.g., *Valet and Meynadier*, 1993; *Meynadier et al.*, 1994; *Guyodo and Valet*, 1999; *Valet et al.*, 2005, and references therein], as does the MB reversal, revealed worldwide by lava lows [*Brown et al.*, 2009], marine and lacustrine sediments [e.g., *Hillhouse and Cox*, 1976; *Valet et al.*, 1988, 1989, 1994; *Channell et al.*, 2004; *Clement and Kent*, 1991; *Schneider et al.*, 1992; *Oda et al.*, 2000; *Yamazaki and Oda*, 2001; *Hyodo et al.*, 2006], and Chinese loess [*Sun et al.*, 1993; *Zhu et al.*, 1993, 1994a]. The directional abnormality is indeed correlated with a low field intensity [*Lund et al.*, 2005], and field directions during a period of low field intensity may be unfaithfully preserved in sediments [*Coe*

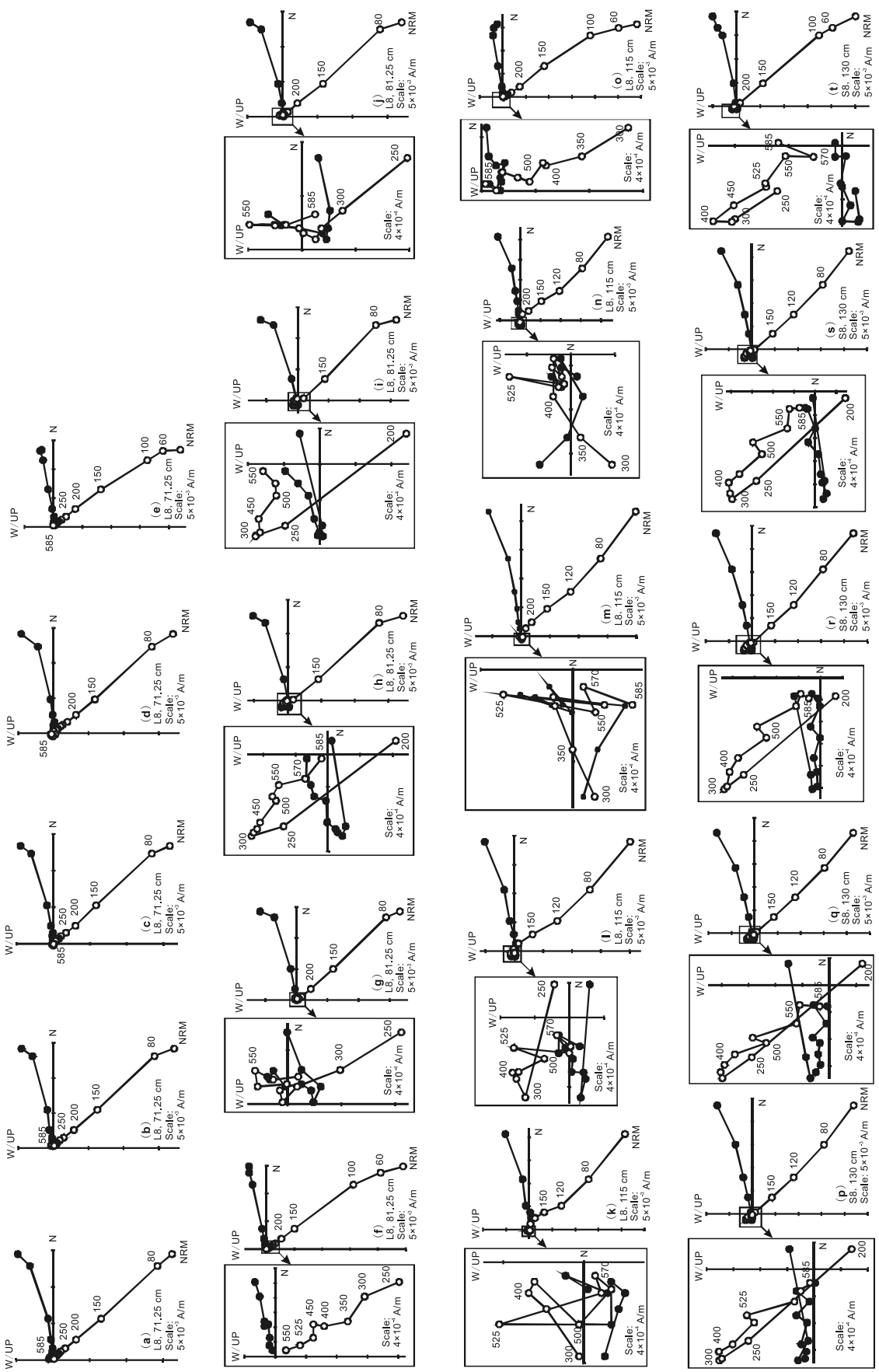

Figure 9. Orthogonal projections of progressive thermal demagnetization of natural remanent magnetization (NRM) for representative (a–e) normal, (f–o) transitional, and (p–t) reverse specimens. Shaded and open circles represent projections onto the horizontal and vertical plane, respectively. Demagnetization temperature is given as degrees Celsius.

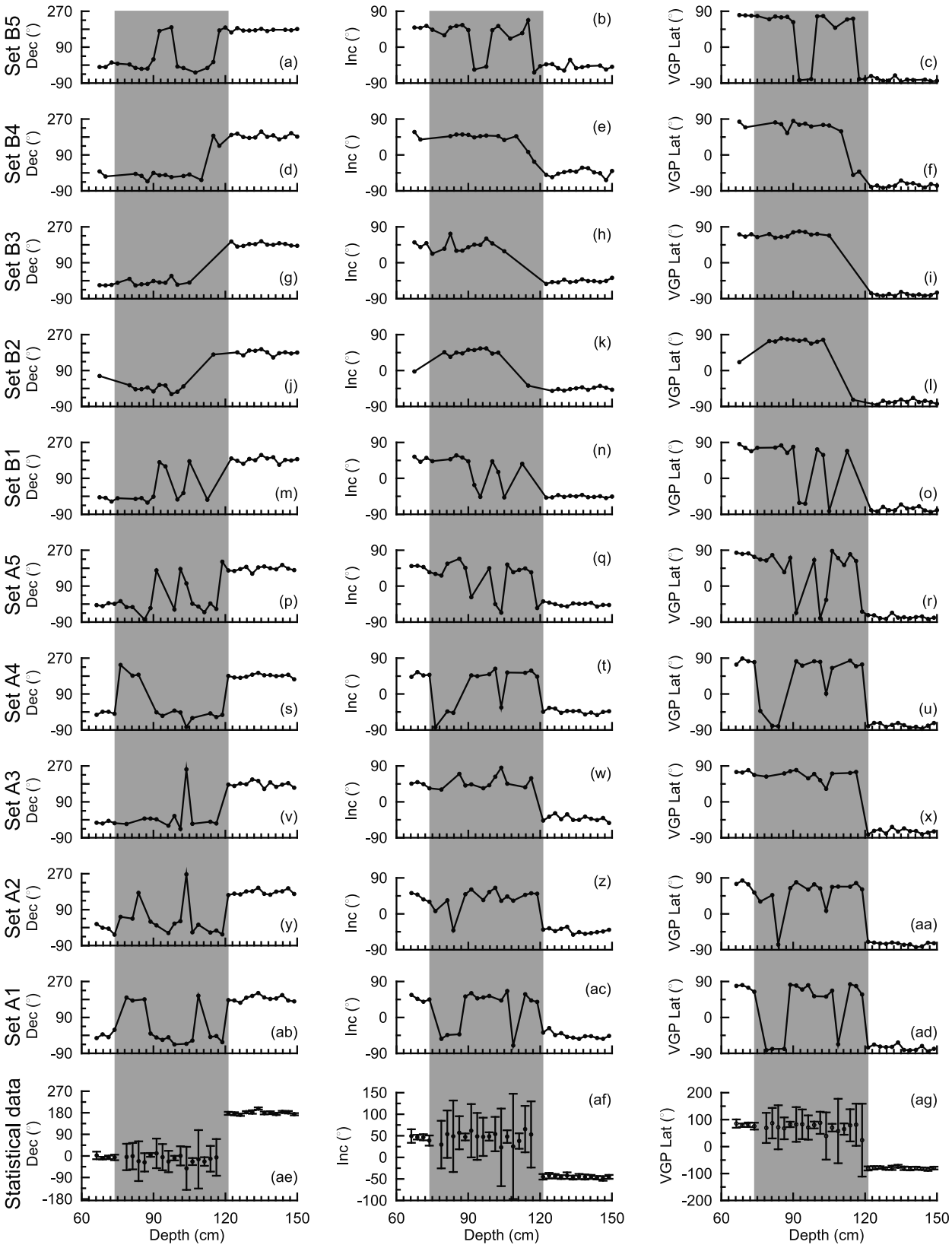

Figure 10. Magnetic stratigraphy of L8 and S8 in the interval 66.25–150 cm. Sets A1–A5 and sets B1–B5 represent parallel specimens. Set B1 is 1.25 cm lower than set A1 along the vertical direction, and sets B2–B5 are 1.25 cm lower than sets A2–A5. Dec, Inc, and VGP Lat are shown in the left, middle, and right columns, respectively. Directional abnormality is shaded. Figures 10ae, 10af, and 10ag are mean ChRMs. Error bars (α_{95}) indicate the dispersion of ChRMs.

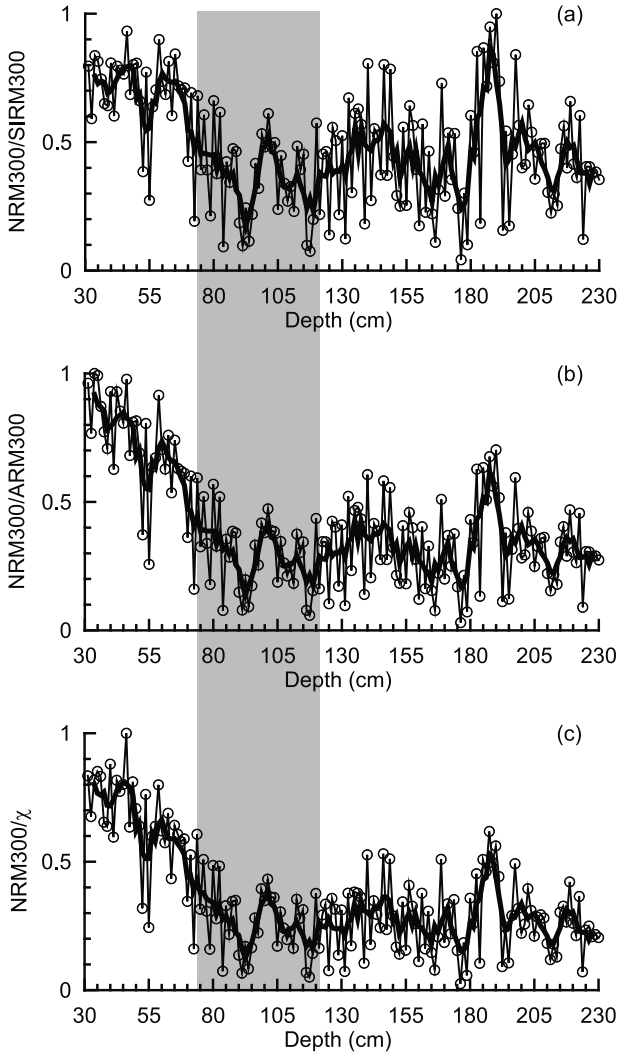

Figure 11. Normalized (a) NRM300/SIRM300, (b) NRM300/ARM300, and (c) NRM300/χ, dependent on depth from 230 to 30 cm. The bold lines represent a three-point running average. NRM300, ARM300, and SIRM300 are residues of NRM, ARM, and SIRM after 300°C thermal treatment, respectively. The shallow RPI corresponds to the transitional interval of paleomagnetic directions. ARM, anhysterestic remanent magnetization; SIRM, saturation IRM.

and Liddicoat, 1994]. At a critical value that is unknown at present, the magnetic field was not powerful enough to efficiently realign the detrital magnetite, resulting in a disorderly and unsystematic distribution of paleomagnetic directions. This model can easily interpret why a large number of samples within the transitional zone did not show stable ChRM. *Coe and Liddicoat* [1994] reexamined the Mono Lake excursion recorded in the Mono Lake area and found that magnetic records during low field intensity may be overprinted by the following stronger field. If this case is applicable to our study, directions during the transitional zone would be more consistent with one another to some extent. However, in Chinese loess, magnetic grains may be cemented in a short period after dust deposition owing to diagenesis. But we must note that pedogenesis after dust accumulation may produce chemical remanent magnetization and lead to partial overprinting of the primary remanent magnetization [*Spassov et al.*, 2003; *Zhu et al.*, 2006]. In this study, pedological evidence demonstrates that pedogenesis increases from L8 to S8. ChRMs are scattered for parallel samples around the transitional zone of L8 and S8, with an interval of 73.75–121.25 cm, but are consistent for parallel samples at the depth interval of 121.25–150 cm in the upper part of S8. This indicates that pedogenesis is irrelevant to the magnetic discrepancies in the MBB.

[37] The other cause for the discrepancies may be linked to the low sediment rate of Chinese loess. *Lund et al.* [2005] correlated four deep-sea sediment records of the Laschamp excursion and documented that smoothing of the NRM would be remarkable to distort recording of paleomagnetic signals under a low sediment rate (<20 cm/ka). In Chinese loess the dust sediment rate is often <20 cm/ka [*Zhu et al.*, 2006]. *Zhu et al.* [2006] also pointed out that, because of the too low sediment rate, the morphological characteristics recorded in the Laschamp excursion in the Luochuan section, Weinan section [*Zhu et al.*, 1999], and Lingtai section [*Zhu et al.*, 2000b] disagree with one another but show a consistent location in stratigraphy and a low-intensity model. Detailed geomagentic signals may have been smeared by the smoothing-in process, so that only the position of the excursion was left [*Zhu et al.*, 2006]. It is obvious that the low sediment rate is a possible cause for the poor paleomagnetic records of Chinese loess during an excursion or a reversal, especially when the true paleomagnetic directions change rapidly. On the contrary, the absence of geomagnetic excursions has been used to indicate the discontinuity of loess deposits at the millennial timescale [*Zhu et al.*, 2007; *Deng*, 2008].

[38] Unlike the transitional field, paleomagnetic directions outside the MBB were well defined, mostly because the field intensity is high enough to align the magnetic particles sufficiently to record consistent signals. Therefore, although it is difficult to obtain reliable transitional signals, the MBB event and its stratigraphic location can still be confidently defined. The stratigraphic location of the MBB is located at the transitional zone between S8 and L8 in the Luochuan section. This is consistent with the recent study by *Liu et al.* [2008] that recorded the MBB at the top of S8 and reported that there is no substantial displacement of the MBB in Chinese loess. Consequently, we also exclude the large lock-in model suggested by *Zhou and Shackleton* [1999], *Heslop et al.* [2000], and *Spassov et al.* [2003]. On the basis of our results, the MBB transitional zone in the Luochuan section is 47.5 cm. If only one or two sets had been used to establish the transitional process, a transitional zone with a thickness in the range of 2.5 to 47.5 cm might have been obtained (shown in Figure 10). Therefore, studies using only one set of samples will surely result in large discrepancies in MBB location.

6. Conclusion

[39] Detailed rock magnetism and paleomagnetism were carried out on samples from L8 and S8 in the Luochuan section, located in the hinterland of the CLP. ChRMs were mainly carried by detrital PSD magnetite of eolian origin. AMS results presented an oblate susceptibility ellipsoid and

revealed undisturbed sediment fabric. Paleomagnetism results for large numbers of subsets of samples show a distinct polarity transitional zone with an interval of 47.5 cm corresponding to low RPI, located in the boundary between L8 and S8. ChRM directions show distinct discrepancies within the MB transitional zone but consistent results outside the transition. We interpret this as low-efficiency alignment of magnetic grains due to the low field intensity during reversal, although the critical value is unknown at present. A low loess sediment rate and limited loess continuity may also reduce faithful recording of the paleomagnetic field. We conclude that the Chinese loess-paleosol sequence can record the exact stratigraphic location of geomagnetic reversal, but the detailed morphology for the transitional field within the reversal is less defined. In addition, a large number of parallel samples should be the standard for further loess studies, to obtain consistent paleomagnetic signals.

[40] **Acknowledgments.** This work was supported by NSFC 40974036 and 40821091 and the 100 Talent Program of the Chinese Academy of Sciences. Paleomagnetic and mineral magnetic measurements were made at the Paleomagnetism and Geochronology Laboratory (SKL-LE), Institute of Geology and Geophysics, Chinese Academy of Sciences.

[41] We gratefully acknowledge two anonymous journal reviewers and the associate editor for their critical comments.

References

Brown, M. C., M. N. Gratton, J. Shaw, R. Holme, and V. Soler (2009), Microwave palaeointensity results from the Matuyama-Brunhes geomagnetic field reversal, *Phys. Earth Planet. Inter.*, *173*, 75–102, doi:10.1016/j.pepi.2008.11.001.

Channell, J. E. T., J. H. Curtis, and B. P. Flower (2004), The Matuyama-Brunhes boundary interval (500–900 ka) in North Atlantic drift sediments, *Geophys. J. Int.*, *158*, 489–505, doi:10.1111/j.1365-246X.2004.02329.x.

Clement, B. M., and D. V. Kent (1991), A southern hemisphere record of the Matuyama-Brunhes polarity reversal, *Geophys. Res. Lett.*, *18*(1), 81–84, doi:10.1029/90GL02714.

Coe, R. S., and J. C. Liddicoat (1994), Overprinting of natural magnetic remanence in lake sediments by a subsequent high-intensity field, *Nature*, *367*(6), 57–59, doi:10.1038/367057a0.

Coe, R. S., B. S. Singer, M. S. Pringle, and X. X. Zhao (2004), Matuyama-Brunhes reversal and Kamikatsura event on Maui: Paleomagnetic directions, $^{40}Ar/^{39}Ar$ ages and implications, *Earth Planet. Sci. Lett.*, *222*, 667–684, doi:10.1016/j.epsl.2004.03.003.

Day, R., M. Fuller, and V. A. Schmidt (1977), Hysteresis properties of titanomagnetite: Grain-size and compositional dependence, *Phys. Earth Planet. Inter.*, *13*, 260–266, doi:10.1016/0031-9201(77)90108-X.

Deng, C. L. (2008), Paleomagnetic and mineral magnetic investigation of the Baicaoyuan loess-paleosol sequence of the western Chinese Loess Plateau over the last glacial-interglacial cycle and its geological implications, *Geochem. Geophys. Geosyst.*, *9*(4), Q04034. doi:10.1029/2007GC001928.

Deng, C. L., R. X. Zhu, K. L. Verosub, M. J. Singer, and B. Y. Yuan (2000), Paleoclimatic significance of the temperature-dependent susceptibility of Holocene loess along a NW-SE transect in the Chinese loess plateau, *Geophys. Res. Lett.*, *27*(22), 3715–3718, doi:10.1029/2000GL008462.

Deng, C. L., R. X. Zhu, K. L. Verosub, M. J. Singer, and N. J. Vidic (2004), Mineral magnetic properties of loess/paleosol couplets of the central loess plateau of China over the last 1.2 Myr, *J. Geophys. Res.*, *109*, B01103, doi:10.1029/2003JB002532.

Deng, C. L., N. J. Vidic, K. L. Verosub, M. J. Singer, Q. S. Liu, J. Shaw, and R. X. Zhu (2005), Mineral magnetic variation of the Jiaodao Chinese loess/paleosol sequence and its bearing on long-term climatic variability, *J. Geophys. Res.*, *110*, B03103, doi:10.1029/2004JB003451.

Deng, C. L., J. Shaw, Q. S. Liu, Y. X. Pan, and R. X. Zhu (2006), Mineral magnetic variation of the Jingbian loess/paleosol sequence in the northern Loess Plateau of China: Implications for Quaternary development of Asian aridification and cooling, *Earth Planet. Sci. Lett.*, *241*(1/2), 248–259, doi:10.1016/j.epsl.2005.10.020.

Ding, Z. L., J. M. Sun, S. L. Yang, and T. S. Liu (1998), Preliminary magnetostratigraphy of a thick eolian red clay-loess sequence at Lingtai, the Chinese Loess Plateau, *Geophys. Res. Lett.*, *25*(8), 1225–1228, doi:10.1029/98GL00836.

Ding, Z. L., J. M. Sun, and T. S. Liu (1999), Stepwise advance of the Mu Us Desert since late Pliocene: Evidence from a red clay-loess record, *Chin. Sci. Bull.*, *44*(13), 1211–1214, doi:10.1007/BF02885968.

Ding, Z. L., E. Derbyshire, S. L. Yang, Z. W. Yu, and S. F. Xiong (2002), Stacked 2.6-Ma grain size record from the Chinese loess based on five sections and correlation with the deep-sea $\delta^{18}O$ record, *Paleoceanography*, *17*(3), 1033, doi:10.1029/2001PA000725.

Dunlop, D. J. (2002), Theory and application of the Day plot (M_{rs}/M_s versus H_{cr}/H_c), 1: Theoretical curves and tests using titanomagnetite data, *J. Geophys. Res.*, *107*(B3), 2056, doi:10.1029/2001JB000486.

Evans, M. E., and F. Heller (2001), Magnetism of loess palaeosol sequences: Recent developments, *Earth Sci. Rev.*, *54*, 129–144, doi:10.1016/S0012-8252(01)00044-7.

Fang, X. M., J. J. Li, R. Van derVoo, C. M. Niocaill, X. R. Dai, R. A. Kemp, E. Derbyshire, J. X. Cao, J. M. Wang, and G. Wang (1997), A record of the Blake Event during the last interglacial paleosol in the western Loess Plateau of China, *Earth Planet. Sci. Lett.*, *146*, 73–82, doi:10.1016/S0012-821X(96)00222-1.

Fisher, R. A. (1953), Dispersion on a sphere, *Proc. R. Soc. London, Ser. A*, *217*, 295–305, doi:10.1098/rspa.1953.0064.

Guo, B., R. X. Zhu, F. Florindo, Y. X. Pan, and L. P. Yue (2001), Pedogenesis affecting the Matuyama-Brunhes polarity transition recorded in Chinese loess, *Chin. Sci. Bull.*, *46*(12), 975–981.

Guo, B., R. X. Zhu, F. Florindo, Z. L. Ding, and J. M. Sun (2002a), A short, reverse polarity interval within the Jaramillo subchron: Evidence from the Jingbian section, northern Chinese Loess Plateau, *J. Geophys. Res.*, *107*(B6), 2124, doi:10.1029/2001JB000706.

Guo, Z. T., W. F. Ruddiman, Q. Z. Hao, H. B. Wu, Y. S. Qiao, R. X. Zhu, S. Z. Peng, J. J. Wei, B. Y. Yuan, and T. S. Liu (2002b), Onset of Asian desertification by 22 Myr ago inferred from loess deposits in China, *Nature*, *416*, 159–163, doi:10.1038/416159a.

Guyodo, Y., and J. P. Valet (1999), Global changes in intensity of the Earth's magnetic field during the past 800 kyr, *Nature*, *399*, 249–252, doi:10.1038/20420.

Heller, F., and M. E. Evans (1995), Loess magnetism, *Rev. Geophys.*, *33*, 211–240, doi:10.1029/95RG00579.

Heller, F., and T. S. Liu (1982), Magnetostratigraphical dating of loess deposits in China, *Nature*, *300*, 431–433, doi:10.1038/300431a0.

Heller, F., and T. S. Liu (1984), Magnetism of Chinese loess deposits, *Geophys. J. R. Astron. Soc.*, *77*, 125–141.

Heller, F., and T. S. Liu (1986), Palaeoclimatic and sedimentary history from magnetic susceptibility of loess in China, *Geophys. Res. Lett.*, *13*(11), 1169–1172, doi:10.1029/GL013i011p01169.

Heller, F., M. Beat, J. D. Wang, H. M. Li, and T. S. Liu (1987), Magnetization and sedimentation history of loess in the central loess plateau of China, in *Aspects of Loess Research*, edited by T. S. Liu, pp. 147–163, China Ocean Press, Beijing.

Heslop, D., C. G. Langereis, and M. J. Dekkers (2000), A new astronomical timescale for the loess deposits of northern China, *Earth Planet. Sci. Lett.*, *184*, 125–139, doi:10.1016/S0012-821X(00)00324-1.

Hillhouse, J., and A. Cox (1976), Brunhes-Matuyama polarity transition, *Earth Planet. Sci. Lett.*, *29*, 51–64, doi:10.1016/0012-821X(76)90025-X.

Hyodo, M., D. K. Biswas, T. Noda, N. Tomioka, T. Mishima, C. Itota, and H. Sato (2006), Millennial- to submillennial-scale features of the Matuyama-Brunhes geomagnetic polarity transition from Osaka Bay, southwestern Japan, *J. Geophys. Res.*, *111*, B02103, doi:10.1029/2004JB003584.

Kirschvink, J. L. (1980), The least-squares line and plane and the analysis of palaeomagnetic data, *Geophys. J. R. Astron. Soc.*, *62*, 699–718.

Larson, E. E., and P. E. Patterson (1993), The Matuyama-Brunhes reversal at Tecopa basin, southeastern California, revisited again, *Earth Planet. Sci. Lett.*, *120*, 311–325, doi:10.1016/0012-821X(93)90247-7.

Levia, S., and S. K. Banerjee (1976), On the possibility of obtaining relative paleointensities from lake sediments, *Earth Planet. Sci. Lett.*, *29*(1), 219–226, doi:10.1016/0012-821X(76)90042-X.

Liu, T. S. (1985), *Loess and the Environment*, 251 pp., China Ocean Press, Beijing.

Liu, Q. S., S. K. Banerjee, and M. J. Jackson (2003), An integrated study of the grain-size-dependent magnetic mineralogy of the Chinese loess/paleosol and its environmental significance, *J. Geophys. Res.*, *108*(B9), 2437, doi:10.1029/2002JB002264.

Liu, Q. S., S. K. Banerjee, M. J. Jackson, C. L. Deng, Y. X. Pan, and R. X. Zhu (2004), New insights into partial oxidation model of magnetites and thermal alteration of magnetic mineralogy of the Chinese loess in air, *Geophys. J. Int.*, *158*, 506–514, doi:10.1111/j.1365-246X.2004.02348.x.

Liu, Q. S., S. K. Banerjee, M. J. Jackson, C. L. Deng, Y. X. Pan, and R. X. Zhu (2005a), Inter-profile correlation of the Chinese loess/paleosol sequences during Marine Oxygen Isotope Stage 5 and indications of pedogenesis, *Quat. Sci. Rev.*, *24*(1/2), 195–210, doi:10.1016/j.quascirev.2004.07.021.

Liu, Q. S., C. L. Deng, Y. Yu, J. Yorrent, M. J. Jackson, S. K. Banerjee, and R. X. Zhu (2005b), Temperature dependence of magnetic susceptibility in an argon environment: Implications for pedogenesis of Chinese loess/palaeosols, *Geophys. J. Int.*, *161*, 102–112, doi:10.1111/j.1365-246X.2005.02564.x.

Liu, Q. S., A. P. Roberts, E. J. Rohling, R. X. Zhu, and Y. B. Sun (2008), Post-depositional remanent magnetization lock-in and the location of the Matuyama-Brunhes geomagnetic reversal boundary in marine and Chinese loess sequences, *Earth Planet. Sci. Lett.*, *275*, 102–110, doi:10.1016/j.epsl.2008.08.004.

Liu, X. M., T. S. Liu, T. C. Xu, C. Liu, and M. Y. Chen (1987), A preliminary study on magnetostratigraphy of a loess profile in Xifeng area, Gansu province, in *Aspects of Loess Research*, edited by T. S. Liu, pp. 164–174, China Ocean Press, Beijing.

Liu, X. M., T. C. Xu, and T. S. Liu (1988), The Chinese loess in Xifeng, II: A study of anisotropy of magnetic susceptibility of loess from Xifeng, *Geophys. J.*, *92*(2), 349–353, doi:10.1111/j.1365-246X.1988.tb01147.x.

Lund, S. P., M. Schwartz, L. Keigwin, and T. Johnson (2005), Deep-sea sediment records of the Laschamp geomagnetic field excursion (~41,000 calendar years before present), *J. Geophys. Res.*, *110*, B04101, doi:10.1029/2003JB002943.

Ma, X. H., Z. S. An, L. P. Yue, S. J. Xu, H. B. Zheng, Y. S. Yan, and D. H. Sun (1991), Preliminary research of B/M transition in Duanjiapo loess section, *Chin. Sci. Bull.*, *36*(16), 1248–1251.

Meynadier, L., J. P. Valet, F. C. Bassinot, N. J. Shackleton, and Y. Guyodo (1994), Asymmetrical saw-tooth pattern of the geomagnetic field intensity from equatorial sediments in the Pacific and Indian Oceans, *Earth Planet. Sci. Lett.*, *126*, 109–127, doi:10.1016/0012-821X(94)90245−3.

Oda, H., H. Shibuya, and V. Hsu (2000), Palaeomagnetic records of the Brunhes/Matuyama polarity transition from ODP Leg 124 (Celebes and Sulu seas), *Geophys. J. Int.*, *142*, 319–338, doi:10.1046/j.1365-246x.2000.00130.x.

Pan, Y. X., R. X. Zhu, J. Shaw, Q. S. Liu, and B. Guo (2001), Can relative paleointensities be determined from the normalized magnetization of the wind-blown loess of China?, *J. Geophys. Res.*, *106*(B9), 19,221–19,232, doi:10.1029/2001JB000360.

Pan, Y. X., R. X. Zhu, Q. S. Liu, B. Guo, L. P. Yue, and H. N. Wu (2002), Geomagnetic episodes of the last 1.2 Myr recorded in Chinese loess, *Geophys. Res. Lett.*, *29*(8), 1282, doi:10.1029/2001GL014024.

Porter, S. C., and Z. S. An (1995), Correlation between climate events in the North Atlantic and China during the last glaciation, *Nature*, *375*, 305–308, doi:10.1038/375305a0.

Rutter, N., Z. L. Ding, M. E. Evans, and T. S. Liu (1991), Baoji-type pedostratigraphic section, loess plateau, north-central China, *Quat. Sci. Rev.*, *10*, 1–22, doi:10.1016/0277-3791(91)90028-S.

Schneider, D. A., D. V. Kent, and G. A. Mello (1992), A detailed chronology of the Australasian impact event, the Brunhes-Matuyama geomagnetic polarity reversal, and global climate change, *Earth Planet. Sci. Lett.*, *111*, 395–405, doi:10.1016/0012-821X(92)90192-X.

Spassov, S., F. Heller, M. E. Evans, L. P. Yue, and Z. L. Ding (2001), The Matuyama/Brunhes geomagnetic polarity transition at Lingtai and Baoji, Chinese Loess Plateau, *Phys. Chem. Earth*, *26*(11/12), 899–904, doi:10.1016/S1464-1895(01)00139-9.

Spassov, S., F. Heller, M. E. Evans, L. P. Yue, and T. von Dobeneck (2003), A lock-in model for the complex Matuyama-Brunhes boundary record of the loess/palaeosol sequence at Lingtai (Central Chinese Loess Plateau), *Geophys. J. Int.*, *155*, 350–366, doi:10.1046/j.1365-246X.2003.02026.x.

Sun, D. H., J. Shaw, Z. S. An, and T. Rolph (1993), Matuyama/Brunhes (M/B) transition recorded in Chinese loess, *J. Geomagn. Geoelectr.*, *45*, 319–330.

Sun, D. H., J. Shaw, Z. S. An, M. Y. Cheng, and L. P. Yue (1998), Magnetostratigraphy and paleoclimatic interpretation of a continuous 7.2 Ma Cenozoic eolian sediments from the Chinese Loess Plateau, *Geophys. Res. Lett.*, *25*(1), 85–88, doi:10.1029/97GL03353.

Tauxe, L. (1993), Sedimentary records of relative paleointensity of the geomagnetic field: Theory and practice, *Rev. Geophys.*, *31*, 319–354, doi:10.1029/93RG01771.

Tauxe, L., A. D. Deino, A. K. Behrensmeyer, and R. Potts (1992), Pinning down the Brunhes/Matuyama and upper Jaramillo boundaries: A reconciliation of orbital and isotopic time scales, *Earth Planet. Sci. Lett.*, *109*, 561–572, doi:10.1016/0012-821X(92)90114-B.

Tauxe, L., T. Pick, and Y. S. Kok (1995), Relative paleointensiitny sediments: A pseudo-Thellier approach, *Geophys. Res. Lett.*, *22*(21), 2885–2888, doi:10.1029/95GL03166.

Tauxe, L., T. Herbert, N. J. Shackleton, and Y. S. Kok (1996), Astronomical calibration of the Matuyama-Brunhes boundary: Consequences for magnetic remanence acquisition in marine carbonates and the Asian loess sequences, *Earth Planet. Sci. Lett.*, *140*, 133–146, doi:10.1016/0012-821X(96)00030-1.

Valet, J. P. (2003), Time variations in geomagnetic intensity, *Rev. Geophys.*, *41*(1), 1004, doi:10.1029/2001RG000104.

Valet, J. P., and L. Meynadier (1993), Geomagnetic field intensity and reversals during the past four million years, *Nature*, *366*, 234–238, doi:10.1038/366234a0.

Valet, J. P., L. Tauxe, and D. R. Clark (1988), The Matuyama-Brunhes transition recorded from Lake Tecopa sediments (California), *Earth Planet. Sci. Lett.*, *87*, 463–472, doi:10.1016/0012-821X(88)90009-X.

Valet, J. P., L. Tauxe, and B. Clement (1989), Equatorial and mid-latitude records of the last geomagnetic reversal from the Atlantic Ocean, *Earth Planet. Sci. Lett.*, *94*, 371–384, doi:10.1016/0012-821X(89)90154-4.

Valet, J. P., L. Meynadier, F. C. Bassinot, and F. Garnier (1994), Relative paleointensity across the last geomagnetic reversal from sediments of the Atlantic, Indian and Pacific Oceans, *Geophys. Res. Lett.*, *21*(6), 485–488, doi:10.1029/93GL02815.

Valet, J. P., L. Meynadier, and Y. Guyodo (2005), Geomagnetic dipole strength and reversal rate over the past two million years, *Nature*, *435*, 802–805, doi:10.1038/nature03674.

Wang, X. S., R. Løvlie, Z. Y. Yang, J. L. Pei, Z. Z. Zhao, and Z. M. Sun (2005), Remagnetization of Quaternary eolian deposits: A case study from SE Chinese Loess Plateau, *Geochem. Geophys. Geosyst.*, *6*(6), Q06H18, doi:10.1029/2004GC000901.

Wang, X. S., Z. Y. Yang, R. Løvlie, Z. M. Sun, and J. L. Pei (2006), A magnetostratigraphic reassessment of correlation between Chinese loess and marine oxygen isotope records over the last 1.1 Ma, *Phys. Earth Planet. Inter.*, *159*, 109–117, doi:10.1016/j.pepi.2006.07.002.

Yamazaki, T., and H. Oda (2001), A Brunhes-Matuyama polarity transition record from anoxic sediments in the South Atlantic (Ocean Drilling Program Hole 1082C), *Earth Planets Space*, *53*, 817–827.

Yang, T. S., M. Hyodo, Z. Y. Yang, and J. L. Fu (2004), Evidence for the Kamikatsura and Santa Rosa excursions recorded in eolian deposits from the southern Chinese Loess Plateau, *J. Geophys. Res.*, *109*, B12105, doi:10.1029/2004JB002966.

Yang, T. S., H. D. Li, J. L. Fu, M. Toshiaki, Z. Y. Yang, and H. Masayuki (2007), Investigation on the lock-in depth of paleosol L_7 and loess L_8 in Baoji (in Chinese with English abstract), *Quat. Sci.*, *27*(6), 972–982.

Yang, T. S., M. Hyodo, Z. Y. Yang, L. Ding, H. D. Li, J. L. Fu, S. B. Wang, H. W. Wang, and T. Mishima (2008), Latest Olduvai short-lived reversal episodes recorded in Chinese loess, *J. Geophys. Res.*, *113*, B05103, doi:10.1029/2007JB005264.

Yue, L. P., Y. Zhou, and Y. Wang (1990), Research of B/M polarity transition at loess section in China (in Chinese with English abstract), *J. Northwest Univ. (Nat. Sci. Ed.)*, *2*, 63–64.

Zheng, H. B., Z. S. An, and J. Shaw (1992), New contributions to Chinese Plio-Pleistocene magnetostratigraphy, *Phys. Earth Planet. Inter.*, *70*, 146–153, doi:10.1016/0031-9201(92)90177-W.

Zheng, H. B., T. Rolph, J. Shaw, and Z. S. An (1995), A detailed palaeomagnetic record for the last interglacial period, *Earth Planet. Sci. Lett.*, *133*, 339–351, doi:10.1016/0012-821X(95)00089-U.

Zhou, L. P., and N. J. Shackleton (1999), Misleading positions of geomagnetic reversal boundaries in Eurasian loess and implications for correlation between continental and marine sedimentary sequences, *Earth Planet. Sci. Lett.*, *168*, 117–130, doi:10.1016/S0012−821X(99)00052−7.

Zhu, R. X., Z. L. Ding, H. N. Wu, B. C. Huang, and L. Jiang (1993), Details of magnetic polarity transition recorded in Chinese loess, *J. Geomagn. Geoelectr.*, *45*, 289–299.

Zhu, R. X., C. Laj, and A. Mazaud (1994a), The Matuyama-Brunhes and Upper Jaramillo transitions recorded in a loess section at Weinan, north-central China, *Earth Planet. Sci. Lett.*, *125*(1/4), 143–158, doi:10.1016/0012-821X(94)90212-7.

Zhu, R. X., L. P. Zhou, C. Laj, A. Mazaud, and Z. L. Ding (1994b), The Blake geomagnetic polarity episode recorded in Chinese loess, *Geophys. Res. Lett.*, *21*(8), 697–700, doi:10.1029/94GL00532.

Zhu, R. X., Y. X. Pan, and Q. S. Liu (1999), Geomagnetic excursions recorded in Chinese loess in the last 70,000 years, *Geophys. Res. Lett.*, *26*(4), 505–508, doi:10.1029/1999GL900019.

Zhu, R. X., B. Guo, Z. L. Ding, and Z. T. Guo (2000a), Gauss-Matuyama polarity transition obtained from a loess section at Weinan, north-central China (in Chinese with English abstract), *Chin. J. Geophys.*, *43*(5), 621–634.

Zhu, R. X., B. Guo, Y. X. Pan, Q. S. Liu, A. Zeman, and V. Suchy (2000b), Reliability of geomagnetic secular variations recorded in a loess section at Lingtai, north-central China, *Sci. China, Ser. D*, *43*(1), 1–9.

Zhu, R. X., Q. S. Liu, Y. X. Pan, C. L. Deng, R. Zhang, and X. F. Wang (2006), No apparent lock-in depth of the Laschamp geomagnetic excursion: Evidence from the Malan loess, *Sci. China, Ser. Earth Sci.*, *49*(9), 960–967.

Zhu, R. X., R. Zhang, C. L. Deng, Y. X. Pan, Q. S. Liu, and Y. B. Sun (2007), Are Chinese loess deposits essentially continuous?, *Geophys. Res. Lett.*, *34*, L17306, doi:10.1029/2007GL030591.

C. Jin and Q. Liu, Paleomagnetism and Geochronology Laboratory, Institute of Geology and Geophysics, Chinese Academy of Sciences, P.O. Box 9825, 19 Beituchengxi Road, Beijing 100029, China. (qsliu@mail.iggcas.ac.cn)